JOURNAL OF MATERIALS SCIENCE 31 (1996) 2301–2310

Microstructure and thermal stability of melt-spun Al–Nd and Al–Ce alloy ribbons

G. WATERLOO*, H. JONES
Department of Engineering Materials, University of Sheffield, Sheffield S1 4DU, UK

Alloys of compositions Al–6Nd, Al–9Ce, Al–16Nd and Al–22Ce (wt%) were prepared by chill-block melt-spinning at a surface speed of $\sim 29\ m\ s^{-1}$ into ribbons of thickness between 20 and 70 μm. The melt-spun ribbons were heat treated for 2 h at 200, 300, 400 and 500 °C. The as-spun and heat-treated ribbons were tested for microhardness and investigated by optical and transmission electron microscopy and X-ray diffraction. Age hardening was not observed for any of the alloys, indicating only a limited amount of extended solid solubility as a result of the melt-spinning conditions used. Al–9Ce and Al–6Nd were found to be relatively stable at a hardness of ~90 HK0.01 and 75–80 HK0.01, respectively, unaffected by heat treatment at up to 300 °C for 2 h, but heat treatment for 2 h at 400 or 500 °C caused softening. Al–6Nd and Al–9Ce as-solidified ribbons comprised a cellular Zone B structure with αAl cells (of size ~0.5 μm) and intercellular orthorhombic $\alpha Al_{11}(Nd, Ce)_3$. The hardness of Al–16Nd as-spun was measured as 330 ± 20 HK0.01 unchanged by heat treatment at 200 °C for 2 h, while heat treatment for 2 h at higher temperatures caused softening. As-spun Al–16Nd consisted of Zone A only comprising αAl solid solution and orthorhombic α or tetragonal $\beta Al_{11}Nd_3$ partly coherent with the matrix. Al–22Ce had a hardness of 330 ± 20 HK0.01 as-spun but softened on treatment for 2 h at 200 °C. As-spun Al–22Ce consisted partly of Zone A structure extending from the wheel side of the ribbon through half of the thickness. The remaining part of the ribbon consisted of cellular Zone B (cell size ~0.2 μm) with intercellular $\alpha Al/\alpha Al_{11}Ce_3$ lamellar eutectic together with areas that were 100% lamellar eutectic (interlamellar spacing 0.09 ± 0.02 μm). All the as-spun microstructures showed coarsening upon heat treatment at sufficiently high temperature. The resulting microstructure after treatment at 500 °C for 2 h consisted of a bimodal distribution of $\alpha Al_{11}(Nd, Ce)_3$ which formed as large particles on the grain boundaries and smaller ones in the grain interiors. The corresponding microstructure was less coarse for Al–16Nd and Al–22Ce.

1. Introduction

When dilute aluminium-based Al–RE (rare-earth) alloys undergo rapid solidification, a combination of characteristics suggests that these alloys should be suitable for high-temperature applications. The high solubility in the liquid state is conducive to extension of solid solubility by rapid solidification and subsequent heat treatment can give rise to dispersion strengthening in these systems. The low equilibrium solid solubility, together with low diffusivity of RE in aluminium, impairs growth of the intermetallic phases formed. The high melting point of these intermetallic dispersoids is a further manifestation of their high stability and suitability for enhancing high-temperature properties.

Systematic investigation of rapidly solidified crystalline Al–RE alloys was begun in the early 1980s by Savage *et al.* [1–5] and continued by Eliezer *et al.* [3–13]. They studied several Al–RE alloys with 10 wt% RE rapidly solidified by the pendant drop melt extraction (PDME) technique. Properties such as thermal stability, oxidation and corrosion behaviour, were studied. Subsequently, in a systematic study of glass-forming ability in chill-block melt-spun ribbons of Al–RE alloys, 20 μm thick, Inoue *et al.* [14–18] found that crystalline αAl-based solid solutions formed at up to 7–9 at% RE were replaced by an amorphous phase with up to 10–17 at% RE, above which unidentified or equilibrium crystalline intermetallic phases began to appear.

The present work is part of an ongoing evaluation of the potential of crystalline Al–RE base alloys as a possible basis of new high-strength thermally stable light alloys. An earlier study reported on the microstructure and response to heat treatment of chill-block melt-spun Al-rich Al–Y [19, 20] and Al–La [19]

Present address: Department of Physics, Norwegian Institute of Technology, University of Trondheim, N-7034 Trondheim, Norway.

0022–2461

TABLE I Nominal compositions of the alloy ingots, together with analysed compositions (1% relative accuracy) and thickness ranges of the melt-spun ribbons obtained

Alloy designation	Alloy ingots	Melt-spun ribbons		
	Nominal composition Ce or Nd	Analysed composition (wt%)	(at%)	Thickness (μm)
Al–9Ce	10	9.0 ± 0.1	1.9 ± 0.0	60 ± 10
Al–22Ce	20	22.4 ± 0.2	5.3 ± 0.1	40 ± 10
Al–6Nd	10	6.2 ± 0.1	1.2 ± 0.0	50 ± 10
Al–16Nd	20	15.9 ± 0.2	3.4 ± 0.0	25 ± 5

alloys. The present work reports corresponding results for alloys of the Al–Nd and Al–Ce systems.

2. Experimental procedure

Alloy ingots each of 30 g of the nominal compositions given in Table I were made from high-purity aluminium (99.996%) and neodymium (99.99%) or cerium (99.99%) by argon arc melting on a cooled copper hearth. The resulting ingots were turned and remelted four times to increase homogeneity. An amount of 4–5 g of each ingot was melt-spun under argon from a quartz crucible on to a copper wheel with a diameter of 0.22 m at a speed of 2500 r.p.m. giving a surface speed of $\sim 29\ m\ s^{-1}$. Optical microscopy of the cross-section of the ingots showed evidence of compositional inhomogeneity. The composition of the melt-spun ribbons was therefore analysed and is also given in Table I together with the ranges of ribbon thickness obtained.

Pieces of ribbon were wrapped in aluminium foil and placed into silica tubes which were evacuated, back-filled with argon and then sealed off. Heat treatments were performed in muffle furnaces with the sample temperature controlled to within ± 3 °C as measured by chromel/alumel thermocouples. The samples were heat treated isochronally for 2 h at 200, 300, 400 and 500 °C after which they were quenched in cold water.

Sections of the ribbons were mounted edge-on in cold-setting resin for optical microscopy and microhardness testing. The microhardness testing was done on a LECO M-400 microhardness machine using a Knoop indentor (HK0.01/15 s) in the centre of the polished cross-section of the ribbon. On each of the as-spun and heat-treated ribbons, 15 measurements were carried out. For optical microscopy the polished ribbon cross-sections were etched in 2.5 M NaOH. Ribbons were also mounted on glass slides using a thin layer of glue, and X-ray diffraction was performed on a Philips 1700 diffractometer with CoK_α radiation. Transmission electron microscopy (TEM) was performed on a Philips 420 instrument at an operating voltage of 120 kV and a Philips CM30 instrument operating at 300 kV. TEM thin foils were prepared by electropolishing in a mixture of 25% HNO_3 and 75% methanol, cooled with liquid nitrogen. Cell sizes of the αAl matrix and interlamellar eutectic spacings were determined by the linear intercept method.

3. Results

3.1. Optical microscopy of the ribbon cross-sections

Optical microscopy of the etched cross-sections of Al–9Ce and Al–6Nd as-spun ribbons showed only Zone B [21] type microstructure consisting of just resolvable microsegregated αAl cells or dendrites with intercellular intermetallic phase. No significant difference between Al–9Ce and Al–6Nd could be detected. Heat treatment at 300 ± 3 °C for 2 h resulted in coarsening via presumed break-up and spherodization of the intercellular intermetallic phase. The cross-sections of Al–22Ce ribbons showed both featureless Zone A [21] and microcellular Zone B structure. Zone A extended from the wheel-cooled surface for a distance one-third to one-half the through-thickness of the ribbon. The Zone A remained featureless when etched after heat treatment at 200 °C for 2 h. Heat treatment for 2 h at 300 °C, or temperatures above, produced coarsening as a result of which it was no longer possible to differentiate between parts of the ribbon that had been Zone A and those that had been Zone B. Optical microscopy of sections of the Al–16Nd ribbons were totally featureless after etching, indicating a Zone A structure through the whole thickness of the ribbon. They remained optically featureless after heat treatment at 200 °C for 2 h. Heat treatment at 300 °C or above resulted in coarsening of the structure, as for Al–22Ce.

3.2. Microhardness

The Knoop microhardness is given as a function of heat-treatment temperature in Table II and Fig. 1. Al–9Ce and Al–6Nd were unchanged at ~ 90 HK0.01 and ~ 70–80 HK0.01, respectively, by heat treatment at 200 or 300 °C for 2 h, but hardness was decreased to ~ 60 HK0.01 by heat treatment at 500 °C for 2 h. For Al–16Nd, microhardness was as high as ~ 330 HK0.01 as-spun and was unchanged by treatment at 200 °C for 2 h, but hardness was decreased by treatment at 300 and 400 °C reaching ~ 90 HK0.01 as a result of treatment at 500 °C for 2 h. Al–22Ce also showed a similar high hardness in the as-spun condition, but was softened to ~ 280 HK0.01 by treatment for 2 h at 200 °C. It continued to soften and reached ~ 100 HK0.01 as a result of treatment at 500 °C for 2 h. The microhardness increased with increasing alloy content (at%) except for Al–16Nd and Al–22Ce of which Al–16Nd possessed the higher hardness.

3.3. X-ray diffraction

XRD traces from Al–9Ce and Al–22Ce as-spun and after heat treatment at 500 °C for 2 h are given in Fig. 2a and b, respectively. These identify the phases present in Al–9Ce and Al–22Ce as-spun to be αAl and α-[22] or β-[23] $Al_{11}Ce_3$. Because of peak broadening it was not possible to distinguish from the data

TABLE II Knoop microhardness with standard deviation measured on ribbon cross-sections (10 g load, 15 s dwell time), both as-spun and after heat treatment at 200–500 °C for 2 h

Alloy	Knoop microhardness ($kg\,mm^{-2}$)				
	As-spun	200 °C/2 h	300 °C/2 h	400 °C/2 h	500 °C/2 h
Al–9Ce	91 ± 7	91 ± 2	87 ± 3	67 ± 5	58 ± 3
Al–22Ce	328 ± 20	284 ± 16	232 ± 9	139 ± 6	101 ± 7
Al–6Nd	74 ± 3	78 ± 3	79 ± 3	66 ± 3	50 ± 3
Al–16Nd	331 ± 22	330 ± 17	210 ± 7	92 ± 8	87 ± 5

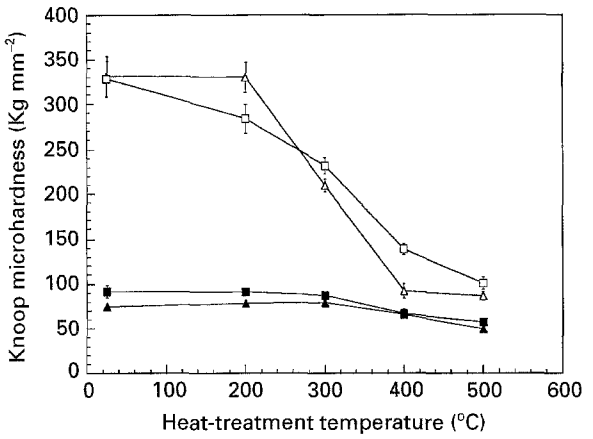

Figure 1 Knoop microhardness (HK0.01/15 s) as a function of temperature of 2 h heat treatment for melt-spun (■) Al–9Ce, (□) Al–22Ce, (▲) Al–6Nd and (△) Al–16Nd.

between the tetragonal high-temperature β and orthorhombic low-temperature α modifications of $Al_{11}Ce_3$ for the as-spun condition. Fig. 2a,b, however, identify the phases present after 2 h at 500 °C as αAl and $\alpha Al_{11}Ce_3$. Similar XRD identified the phases present in Al–6Nd and Al–16Nd as αAl and α-[24] or β-[25] $Al_{11}Nd_3$ for the as-spun condition and αAl plus the orthorhombic low-temperature modification $\alpha Al_{11}Nd_3$ after 2 h at 500 °C.

The αAl lattice parameters of the Al–6Nd and Al–9Ce ribbons both as-spun and after 2 h at 500 °C are compared in Table III with the value for pure annealed αAl [26]. These results indicate that neodymium and cerium in solid solution as-spun gave rise to a small increase in lattice parameter which is reduced somewhat by treatment for 2 h at 500 °C. Strong texture/preferred growth orientation and peak broadening prevented accurate measurements of the lattice parameters of Al–22Ce and Al–16Nd. Al–9Ce and Al–6Nd showed no sign of a preferred growth orientation.

3.4. Transmission electron microscopy

TEM investigations of as-spun Al–6Nd ribbons confirmed the Zone B structure indicated by optical microscopy with αAl cells (size 0.5 ± 0.1 μm) and intercellular $Al_{11}Nd_3$ of thickness approximately 50 nm. This $Al_{11}Nd_3$ was determined by electron diffraction to be the orthorhombic α-modification. Fig. 3a shows a TEM bright-field (BF) micrograph of the structure

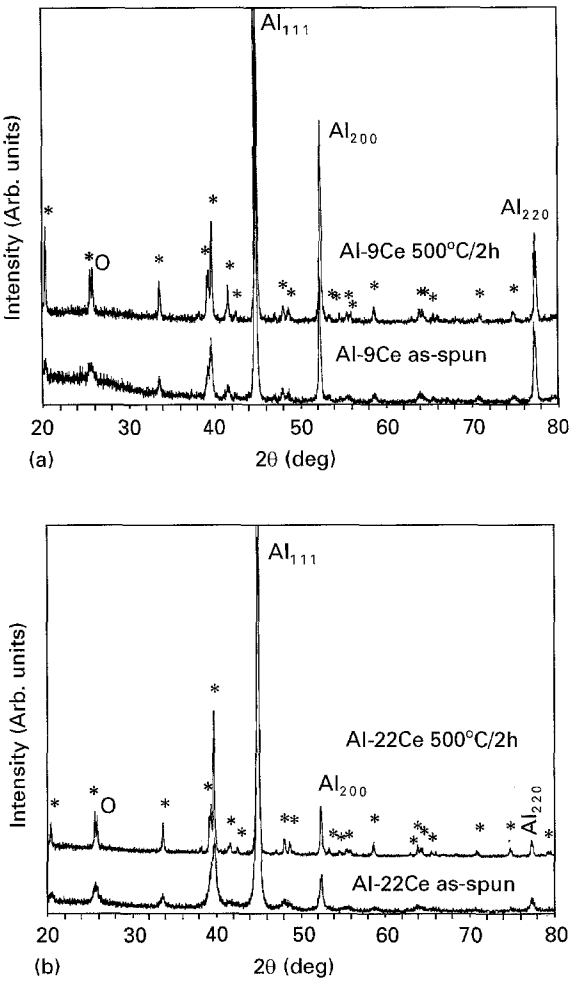

Figure 2 XRD traces for Al–Ce alloy ribbons as-spun and after heat treatment at 500 °C for 2 h: (a) Al–9Ce, (b) Al–22Ce. (*) $Al_{11}Ce_3$ (α/β), (O) α-$Al_{11}Ce_3$ (031).

TABLE III Lattice parameter of αAl at 25 °C in Al–6Nd and Al–9Ce ribbons as-spun and after heat treatment at 500 °C for 2 h, compared with the value for pure annealed aluminium

Alloy	Condition	Lattice parameter (nm)
Pure aluminium	Annealed	0.404 96 ± 0.000 01 [26]
Al–6Nd	As-spun	0.405 06 ± 0.000 02
Al–6Nd	500 °C/2 h	0.405 02 ± 0.000 02
Al–9Ce	As-spun	0.405 04 ± 0.000 04
Al–9Ce	500 °C/2 h	0.405 01 ± 0.000 02

and Fig. 3b shows electron diffraction patterns of $\alpha Al_{11}Nd_3$ [3 $\bar{1}$ 1] and [3 $\bar{1}$ 0] zone axes. The microstructure of Al–9Ce was very similar with αAl cell size 0.7 ± 0.1 μm. The intercellular intermetallic was also determined to be the orthorhombic low-temperature modification, $\alpha Al_{11}Ce_3$. After heat treatment at 500 °C for 2 h, both alloys showed a bimodal distribution of $\alpha Al_{11}X_3$ (X = Ce or Nd) precipitates with large (~ 0.5 μm) precipitates at the αAl grain boundaries and smaller (0.02–0.2 μm) ones inside the grains. A TEM BF micrograph of Al–6Nd shows this in Fig. 4.

The as-spun Al–22Ce ribbons featured Zone A on the chill side and Zone B in the remainder of the section. Zone A is shown in Fig. 5a. The grains are "star" shaped with small orientation differences within

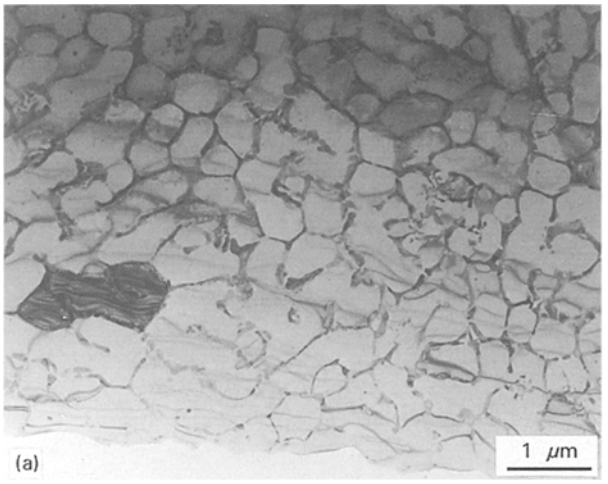

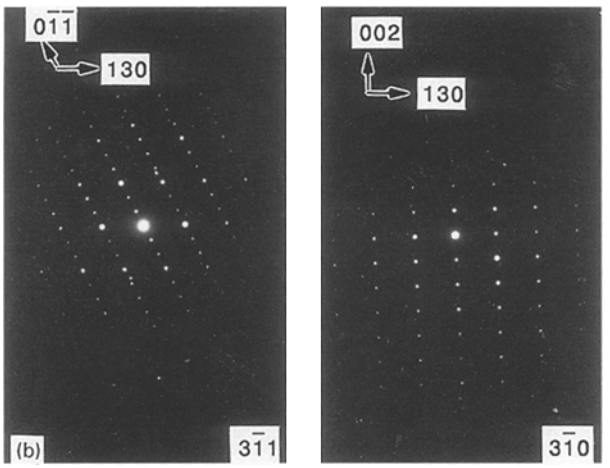

Figure 3 (a) TEM BF micrograph of Zone B in as-spun Al–6Nd showing cellular αAl cells with intercellular $\alpha Al_{11}Nd_3$; (b) electron diffraction patterns of $\alpha Al_{11}Nd_3$ $[3\bar{1}1]$ and $[3\bar{1}0]$ zone axes.

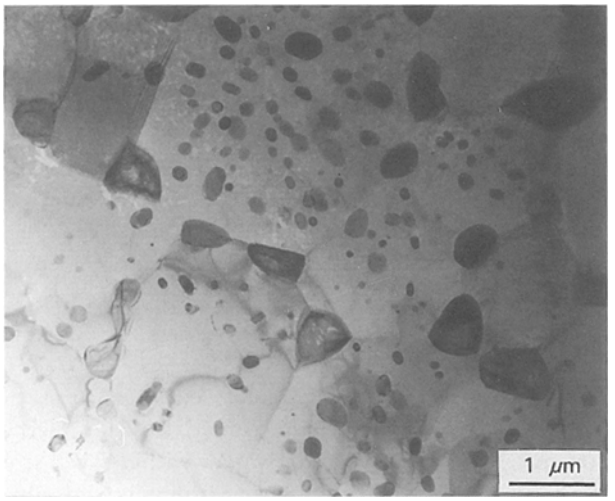

Figure 4 TEM BF micrograph of Al–6Nd ribbon heat treated at 500 °C for 2 h showing a coarsened structure with large $\alpha Al_{11}Nd_3$ particles on the grain boundaries and smaller ones within the grain interiors.

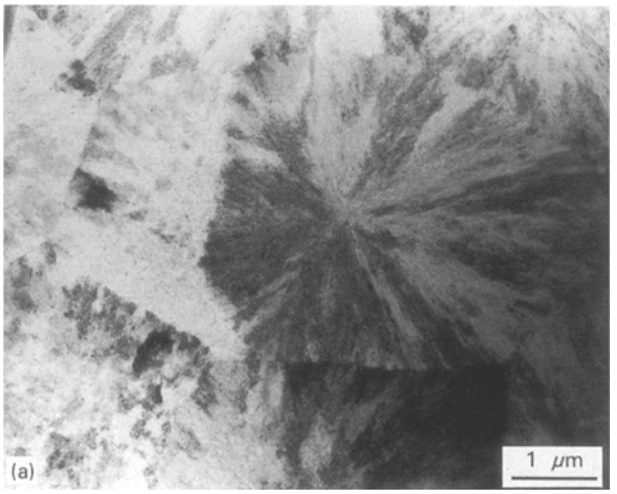

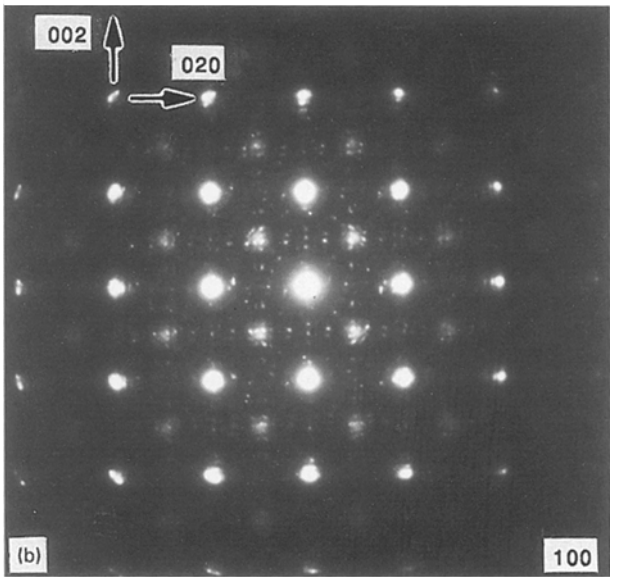

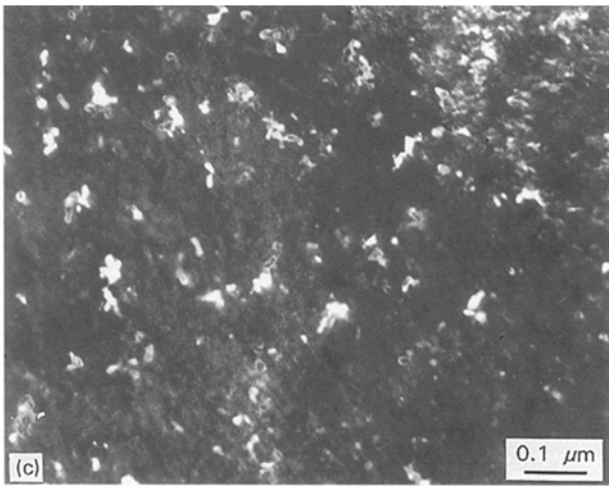

Figure 5 (a) TEM BF micrograph of as-spun Al–22Ce showing Zone A structure with "star" shaped grains; (b) electron diffraction pattern from one of the grains showing αAl ⟨1 0 0⟩ zone axis; (c) DF micrograph of the diffuse reflection in the extinct {1 1 0} αAl showing intermetallic precipitates.

one grain and a grain size of ~1.5–3 μm. Fig. 5b shows an electron diffraction pattern from one of the grains in Fig. 5a. The strong reflections are from the αAl ⟨1 0 0⟩ zone axis. The remaining, more complex, part of the diffraction pattern arises from $Al_{11}Ce_3$ including double scattering. Fig. 5c shows a dark-field (DF) micrograph using the diffuse reflection at the {1 1 0} αAl position which is extinct for aluminium. Consequently, the bright particles in Fig. 5c must be intermetallic particles. Zone B has an αAl cell size ~0.20 ± 0.05 μm with a substantial fraction of

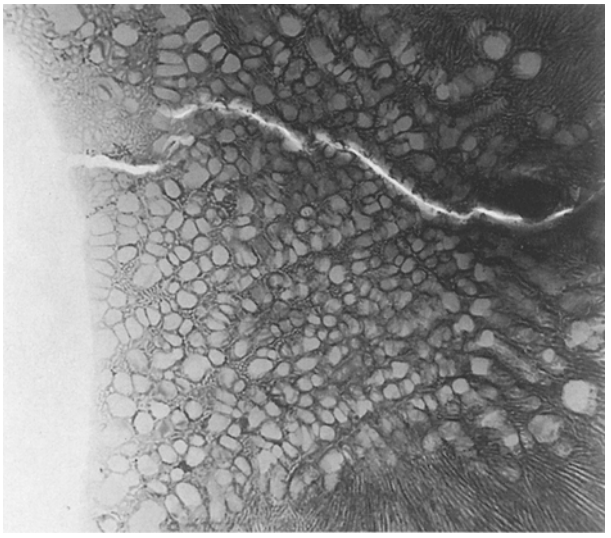

Figure 6 TEM BF micrograph of Al–22Ce as-spun showing cellular Zone B structure with intercellular eutectic of αAl and $\alpha Al_{11}Ce_3$.

intercellular eutectic as shown in Fig. 6. Some areas comprised 100% lamellar eutectic of αAl and $\alpha Al_{11}Ce_3$ as shown in Fig. 7a. The interlamellar spacing was 0.09 ± 0.02 μm. Fig. 7b shows electron diffraction patterns identifying the intermetallic phase as $\alpha Al_{11}Ce_3$. Fig. 7c shows an electron diffraction pattern of the eutectic structure where the orientation relationship $\langle 0\,0\,1\rangle$ Al‖ [0 1 0]$\alpha Al_{11}Ce_3$ and $\{2\,0\,0\}$ Al‖ (0 0 2) $\alpha Al_{11}Ce_3$ has been determined.

Al–16Nd ribbons comprised only the Zone A structure which was very similar to the structure of Zone A in Al–22Ce ribbons. Fig. 8a shows a low-magnification BF micrograph of Zone A grains. Fig. 8b shows the electron diffraction pattern from one of these grains. The strong reflections are from the αAl $\langle 1\,1\,0\rangle$ zone axis. The weaker, diffuse reflections fit well with *d*-values from $\alpha Al_{11}Nd_3$ but the corresponding angles do not fit. Consequently, it is not possible to identify this pattern as one of the zone axes of $\alpha Al_{11}Nd_3$. Fig. 8c shows a high-resolution (HRTEM) micrograph taken with the objective aperture using the weak intermetallic reflections. A series of DF micrographs from the weak intermetallic reflections marked 1, 2 and 3 in Fig. 8b show different bright particles indicating that the reflections in Fig. 8b come from different particles. An example is given in Fig. 8d which is the DF micrograph from reflection 3. The DF micrographs from reflections 1 and 3 show particles of size ~ 1–10 nm while DF of reflection 2 show only the smaller sized particles ~ 1nm or less. Reflection 2 is more diffuse than 1 and 3 which could arise from the distribution of very small particles.

TEM studies of Al–22Ce ribbons heat treated at 200 °C for 2 h did not show significant changes in structure, but coarsening occurred on treatment at 300 °C or above. Fig. 9 shows a TEM BF micrograph of ribbon after heat treatment at 500 °C for 2 h. Similarly, for Al–16Nd the Zone A structure survived heat treatment for 2 h at 200 °C. Heat treatment at higher temperature produced coarsening as for Al–22Ce resulting after 2 h at 500 °C in a microstructure similar to that in Fig. 9 for Al–22Ce. The coarsened precipitates were identified as $\alpha Al_{11}Nd_3$.

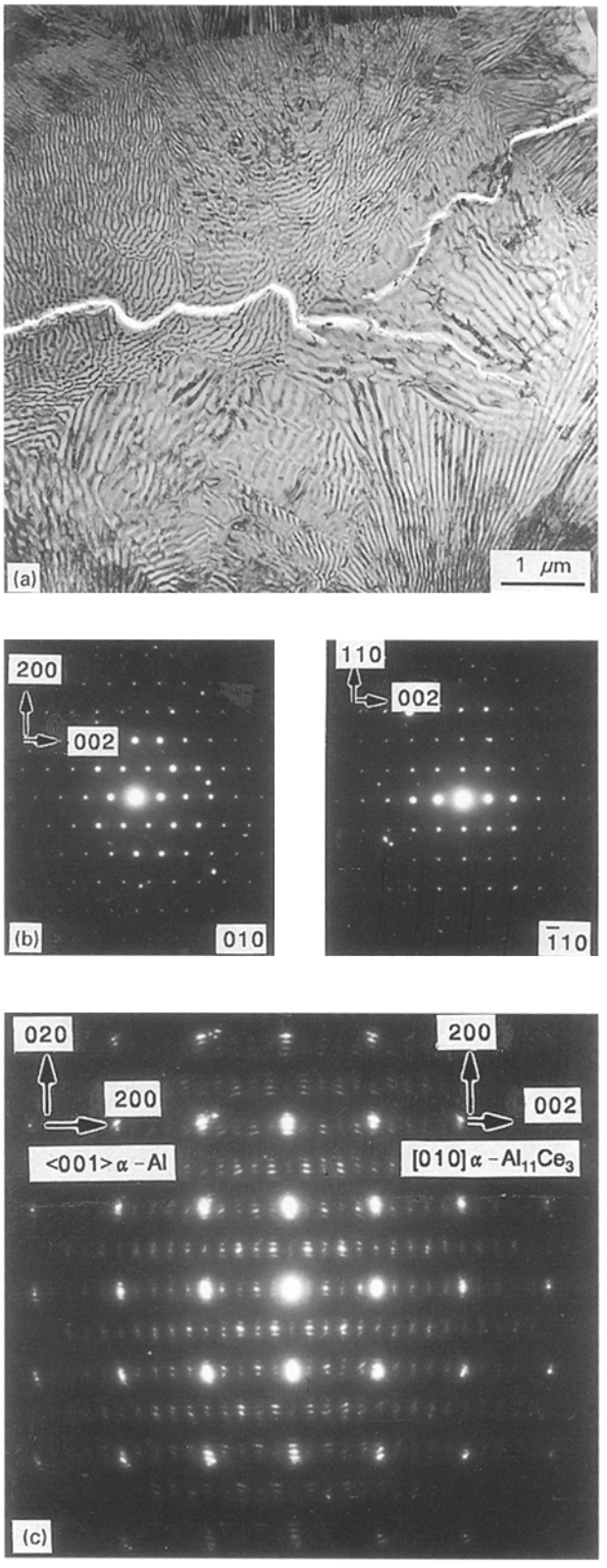

Figure 7 (a) TEM BF micrograph of Al–22Ce as-spun showing a lamellar eutectic of αAl and $\alpha Al_{11}Ce_3$; (b) electron diffraction patterns of $\alpha Al_{11}Ce_3$ [0 1 0] and [$\bar{1}$ 1 0] zone axes; (c) electron diffraction pattern of eutectic $\langle 0\,0\,1\rangle$ αAl ‖ [0 1 0] $\alpha Al_{11}Ce_3$ zone axis.

4. Discussion

4.1. Constitution as-spun

Rapid solidification by chill-block melt-spinning of Al–6Nd, Al–16Nd, Al–9Ce and Al–22Ce (wt %) at a surface speed of ≈ 29 m s^{-1} produced the equilibrium

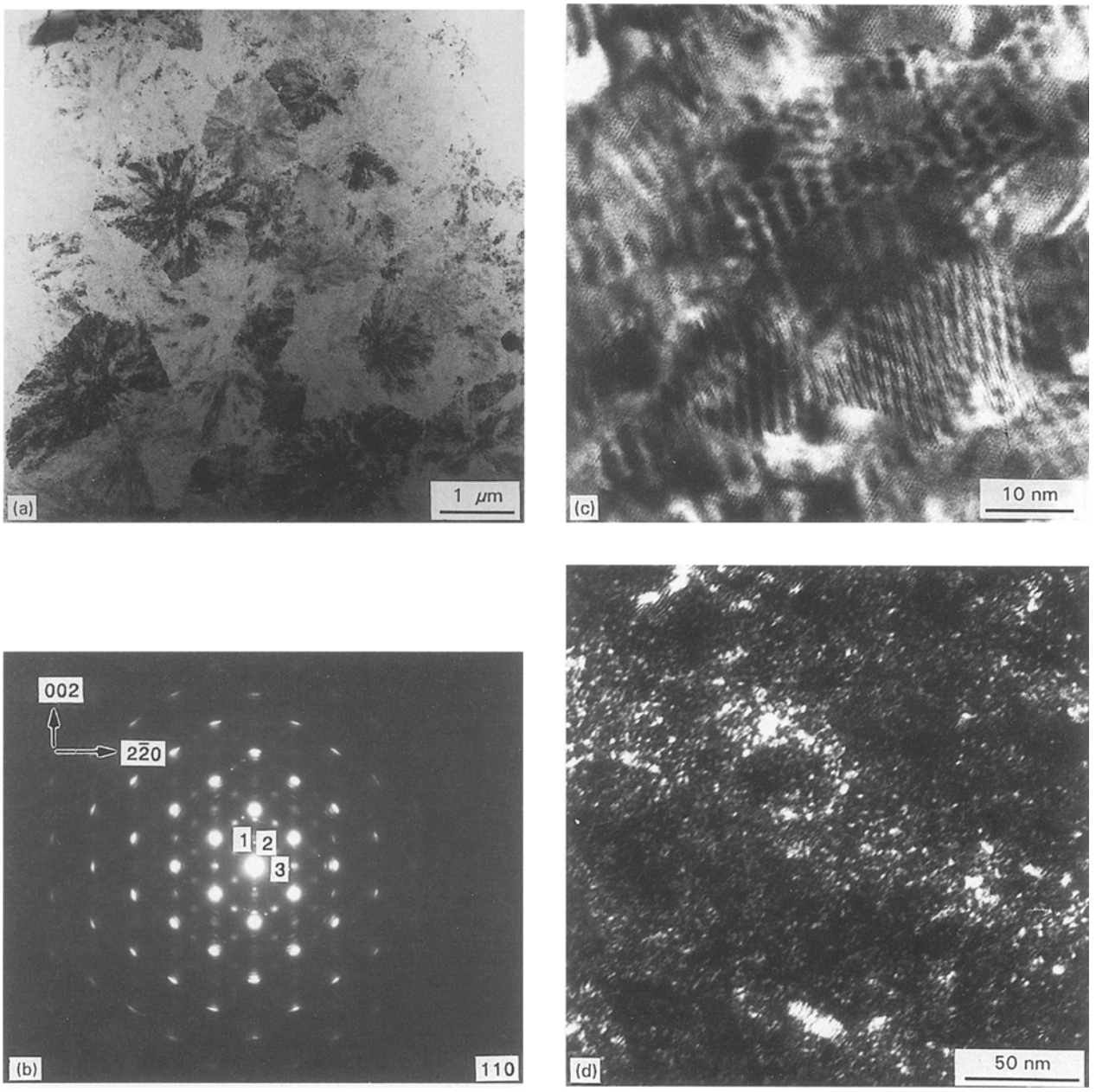

Figure 8 (a) TEM BF micrograph of Al–16Nd as-spun showing "star" shaped Zone A grains; (b) electron diffraction pattern from one of the grains, αAl ⟨1 1 0⟩ zone axis; (c) HRTEM micrograph showing lattice fringes and Moiré patterns from the same zone axis; (d) DF micrographs from the weak intermetallic reflection 3.

phases αAl and $Al_{11}X_3$ (X = Nd or Ce). The small increase in αAl lattice parameter of 0.000 08 ± 0.000 04 nm for Al–9 wt% Ce (1.9 at% Ce) compared with that for pure aluminium in Table III is similar to that recorded by Ning *et al.* [27] for splat-quenched Al–0.2 and 0.5 at% Ce, 50 ± 10 μm thick. Their conclusion was that no more than 0.2 at% Ce or 0.3 at% Nd was retained in solid solution in αAl for their conditions, which is consistent with our findings. With the exception of Al–Eu, Ning *et al.* found a nearly linear increase in extended αAl solid solubility limit with increase in atomic number along the RE series, starting at 0.15 at% for lanthanum and reaching a maximum of 0.75 at% for erbium, reflecting the continuous decrease in atomic radius of the RE addition from 0.208 nm for lanthanum to 0.194 nm for erbium compared with 0.158 nm for aluminium. The strong texture and peak broadening which prevented accurate measurement of the lattice parameter of αAl in as-spun Al–16Nd and Al–22Ce were not reported by Dill *et al.* [19] for otherwise comparable as-spun Al–18.2 wt% Y and Al–18.4 wt% La. The line broadening for our samples could possibly be associated with larger compositional variations within the αAl in the "star" shaped grains than were presented for Al–18Y or Al–18La. The conclusion from our work that α or β $Al_{11}X_3$ (X = Ce or Nd) formed as the second phase in the as-spun condition is in line with the earlier findings [19, 20] for Al–Y and Al–La. As for Al–La, $Al_{11}X_3$ is the equilibrium second phase for Al-rich alloys of the Al–Ce [28] and Al–Nd [29, 30] systems, as appears to be the case for all Al–RE systems from Al–La through to Al–Eu, beyond which some form of Al_3RE becomes the equilibrium second phase [31]. Our firm identification that the $Al_{11}Ce_3$ present in intercellular and eutectic regions of Zone B in Al–22Ce is the orthorhombic low-temperature α-modification contrasts with the finding [20] that the

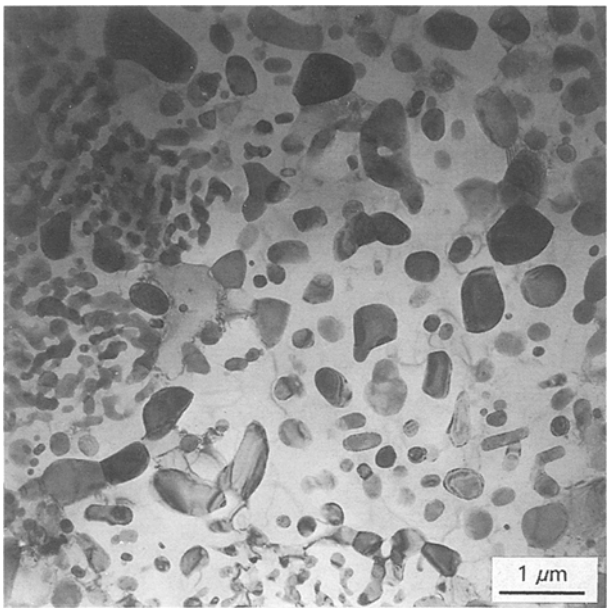

Figure 9 TEM BF micrograph of the Al–22Ce ribbon heat treated at 500 °C/2 h showing a coarsened structure of $\alpha Al_{11}Ce_3$ particles in an αAl matrix.

comparable intercellular phase in as-spun Al–10Y was the tetragonal β-modification.

4.2. Microstructure as-spun

Optical microscopy of ribbon cross-sections after etching showed that Al–6Nd and Al–9Ce consisted of Zone B only. Savage and Froes [1], Eliezer *et al.* [4] and Fass and Eliezer [11] reported both Zone A and Zone B in PDME ribbons of Al–10.7 wt% Nd [1], Al–10.7 wt% Nd and Al–9.8 wt% Ce [4] and Al–10.3 wt% Ce [11] which are comparable alloys. The part of Zone B for Al–10.7 wt% Nd [8] investigated by TEM was reported to consist of grains (size 2–3 μm) with spherical precipitates inside (size ~0.2 μm) and precipitate-free zones at the grain boundaries. This is different from the cellular structure found here. Zone A of PDME Al–10.7 wt% Nd and Al–9.8 wt% Ce was investigated by TEM [4]. A cellular structure with cell size 0.5–2.5 μm and intercellular eutectic was reported. This is consistent with the Zone B structure found in our work.

Increasing the alloying content to Al–16 wt% Nd and Al–22 wt% Ce gave rise to complete or partial change from Zone B to Zone A structure. TEM investigations confirmed the results from optical microscopy for Al–16Nd showing only Zone A with "star" shaped αAl grains with small intermetallic precipitates. For Al–22Ce optical microscopy indicated both Zone A and Zone B structures. TEM showed the same Zone A structure as for Al–16Nd and Zone B consisting of αAl dendrites plus interdendritic $\alpha Al/\alpha Al_{11}Ce_3$ eutectic. In addition there were regions comprising lamellar $\alpha Al/\alpha Al_{11}Ce_3$ eutectic alone. Change from Zone B to Zone A structures with increasing alloying content was also reported by Dill *et al.* [19] for Al–Y and Al–La alloys. The Zone A structure can be characterized as a microsegregation-free or microcellular-extended solid solution. In general, the critical growth velocity or undercooling necessary for producing a microsegregation-free or microcellular solid solution can decrease at sufficiently high alloying content [32, 33] fully consistent with our observations.

Microstructural scale parameters such as cell size and eutectic interphase spacing as-spun can be used to estimate applicable cooling rates and solidification front velocities. The relevant cell-size measurements for Zone B in Al–6Nd, Al–9Ce and Al–22Ce are given in Table IV together with measured eutectic spacing for the eutectic areas in Al–22Ce. Cooling rates, $\dot{T}$, corresponding to the Zone B cell sizes are 1×10^6 and 4×10^5 K s^{-1} for Al–6Nd and Al–9Ce, respectively, and 2×10^7 K s^{-1} for Al–22Ce. Assuming that newtonian conditions applied, then [34]

$$\dot{T} = \frac{h(T - T_A)}{c\rho z} \quad (1)$$

where h is the heat transfer coefficient, T the sample temperature, T_A the ambient temperature, c the specific heat, ρ the density and z the thickness of the sample, from which

$$h = c\rho z\dot{T}/(T - T_A) \quad (2)$$

Taking c as 900 J kg^{1}K^{-1} and ρ as 2.7 Mg m^{-3} for aluminium [35], and $T - T_A$ as 600 K gives operative h-values of 0.1–2 W mm^{-2} K^{-1} very typical of chill-surface rapid-solidification processes [34]. Using $\Lambda R^{1/2} = 12\ \mu m^{3/2} s^{-1/2}$ from measurements by Street *et al.* [36] for the $\alpha Al/Al_{11}Ce_3$ eutectic, where Λ is eutectic spacing and R is growth velocity, gives $R = 20 \pm 10$ mm s^{-1} for the values of Λ in Table IV. Again assuming that newtonian conditions apply

$$R = \frac{h(T_F - T_A)}{L\rho} \quad (3)$$

where T_F is the solidification temperature and L is the latent heat of solidification, from which

$$h = L\rho R/(T_F - T_A) \quad (4)$$

Taking L as 330 kJ kg^{-1} and ρ as 2.7 Mg m^{-3} for aluminium [35] and $T_F - T_A$ as 600 K gives $h \sim 0.03 \pm 0.015$ W mm^{-2} K^{-1}, somewhat smaller than from the corresponding αAl cell-size measurements.

4.3. Effects of heat treatment on microstructure

Both Zone A and Zone B regions showed no indication of microstructural change as a result of 2 h exposure to 200 °C, while increased spheroidization and coarsening evidently occurred in 2 h treatments at 300, 400 and 500 °C. This is broadly in line with the behaviour of comparable Al–Y and Al–La samples [19], with the difference that the transformation of $Al_{11}X_3$ into Al_3X found for Al–20Y did not occur for Al–Ce or Al–Nd (or in Al–La) because $Al_{11}X_3$ is the stable second phase in these systems. It is also notable that the coarsened $Al_{11}X_3$ obtained in Al–6 and 16Nd and in Al–9 and 22Ce after 2 h at 500 °C was again the orthorhombic α-modification found also in the

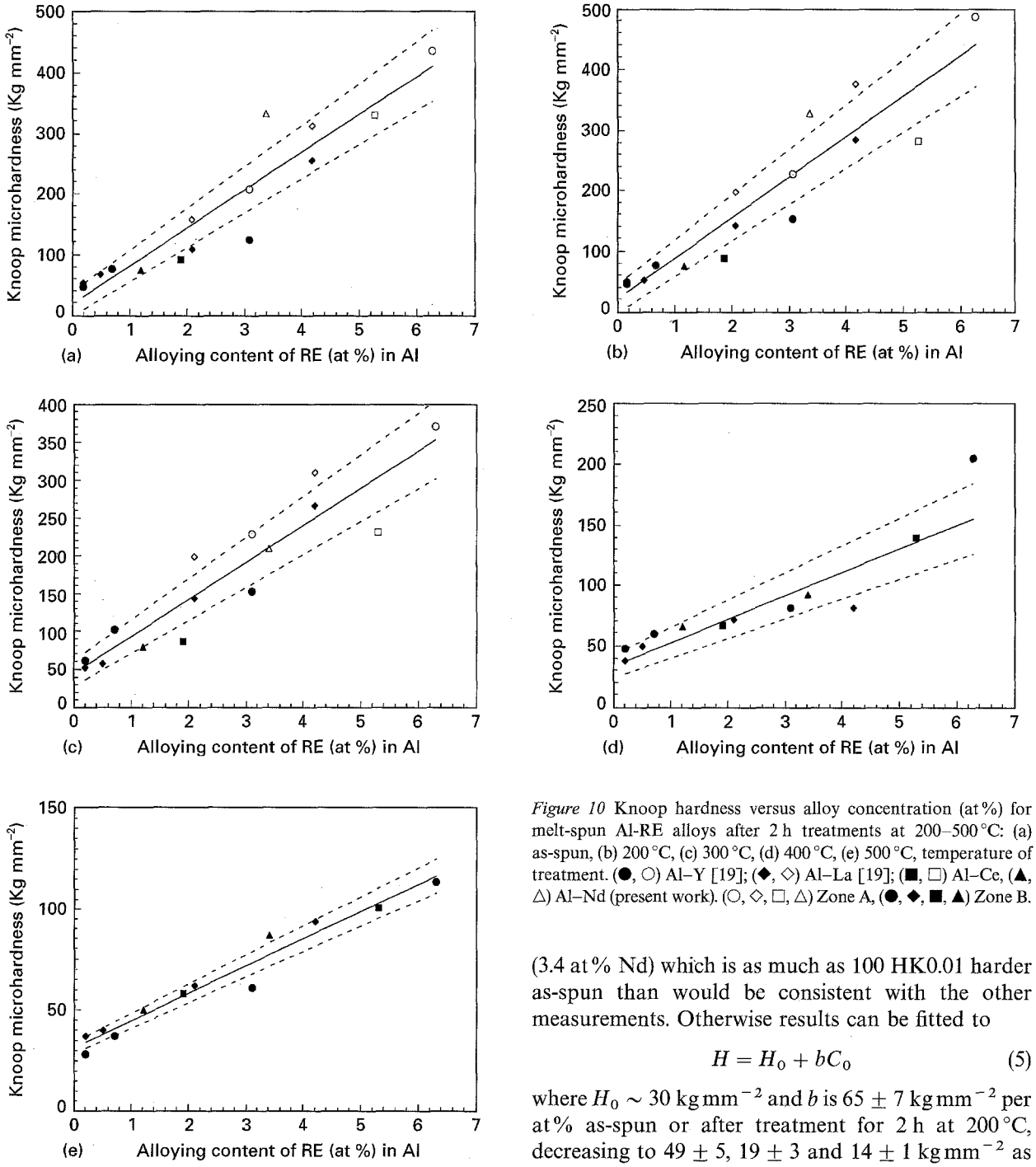

Figure 10 Knoop hardness versus alloy concentration (at%) for melt-spun Al-RE alloys after 2 h treatments at 200–500 °C: (a) as-spun, (b) 200 °C, (c) 300 °C, (d) 400 °C, (e) 500 °C, temperature of treatment. (●, ○) Al–Y [19]; (◆, ◇) Al–La [19]; (■, □) Al–Ce, (▲, △) Al–Nd (present work). (○, ◇, □, △) Zone A, (●, ◆, ■, ▲) Zone B.

as-spun condition for Zone B in Al–6Nd, Al–9Ce and Al–22Ce. This identification was based mainly on the relative positions of the (1 0 1) and (0 3 1) lines in the XRD traces. The *d*-spacing for 0 3 1 is a unique feature of the orthorhombic modification of $Al_{11}X_3$.

4.4. Microhardness results

The microhardness in the as-spun ribbons increased with increasing alloying content. Fig. 10a–e show HK0.01 versus atomic per cent rare-earth from the present work combined with the earlier results of Dill *et al.* [19] for Al–La and Al–Y, both as-spun and after 2 h treatments at 200, 300, 400 and 500 °C. The present results are generally consistent with the earlier data except for the hardness of Zone A in Al–16Nd (3.4 at% Nd) which is as much as 100 HK0.01 harder as-spun than would be consistent with the other measurements. Otherwise results can be fitted to

$$H = H_0 + bC_0 \quad (5)$$

where $H_0 \sim 30\ \mathrm{kg\,mm^{-2}}$ and b is $65 \pm 7\ \mathrm{kg\,mm^{-2}}$ per at% as-spun or after treatment for 2 h at 200 °C, decreasing to 49 ± 5, 19 ± 3 and $14 \pm 1\ \mathrm{kg\,mm^{-2}}$ as a result of treatment for 2 h at 300, 400 or 500 °C.

Age hardening was not observed in any of the present alloys consistent with little extension of αAl solid solubility. The microhardness of Al–6Nd and Al–9Ce ribbon cross-sections was found to be unchanged at ~75–80 HK0.01 and ~90 HK0.01, respectively, by 2 h heat treatments at 200 or 300 °C but hardness was decreased by treatments at 400 and 500 °C. This is generally consistent with the hardness data reported by Savage and Froes [1] for Al–10.7 wt% Nd after 1 h heat treatment in the same temperature interval. For Al–9.8 wt% Ce [4] age hardening with a peak hardness in Zone A of 110 HK0.005 after 1 h at 350 °C was reported. No such age-hardening effect was observed in the present study.

Although our Al–16Nd and Al–22Ce did not show any age hardening effect, Dill *et al.* [19] found a small age-hardening effect for Al–18.2 wt% Y and

TABLE IV Zone B αAl cell size, λ, and $\alpha Al/\alpha Al_{11}Ce_3$ eutectic interphase spacing, Λ, from transmission electron micrographs together with corresponding values of cooling rate, $\dot{T}$, front velocity, R, and heat transfer coefficient, h

Alloy	λ (μm)	z (μm)	$\dot{T}$[a] ($K^{-1}s$)	h ($W\,mm^{-2}K^{-1}$)	Λ (μm)	R[b] ($mm\,s^{-1}$)	h ($W\,mm^{-2}K^{-1}$)
Al–6Nd	0.5 ± 0.1	40 ± 10	1×10^6	0.2	–	–	–
Al–9Ce	0.7 ± 0.1	50 ± 10	4×10^5	0.1	–	–	–
Al–22Ce	0.2 ± 0.05	25 ± 5	2×10^7	2.0	0.09 ± 0.02	20	0.03

[a] $\dot{T}$ determined from $\lambda \dot{T}^{1/3} = 50\,\mu m(K\,s^{-1})^{1/3}$ [21] typical of aluminium alloys with corresponding h from Equation 2.
[b] R determined from $\Lambda R^{1/2} = 12\,\mu m^{3/2}s^{-1/2}$ from measurements from [36] for $\alpha Al/\alpha Al_{11}Ce_3$ eutectic with corresponding h from Equation 4.

Al– 18.4 wt %La. The hardness in our as-spun ribbons was 330 ± 20 HK0.01 for Al–16Nd and 330 ± 20 HK0.01 for Al–22Ce. These values are comparable to the hardness value (310 ± 20 HK0.01) reported by Dill *et al.* [19] for Zone A in Al–18.4 wt% La. For Al–22Ce there was a mixture of Zones A and B present and the ribbons were too narrow for measurements to be made in the separate zones. For Al–16Nd ribbons which consisted of only Zone A the hardness was stable on treatment at 200 °C for 2 h then rapidly decreased to a final value of 87 ± 5 HK0.01 on treatment at 500 °C for 2 h. Al–22Ce decreased in hardness to 101 ± 7 HK0.01 on treatment at 500 °C for 2 h.

5. Conclusions

1. Chill-block melt-spinning of Al–6Nd, Al–16Nd, Al–9Ce and Al–22Ce (wt%) alloys at a speed of $29\,m\,s^{-1}$ produced the equilibrium phases, αAl and $Al_{11}X_3$ (X = Ce or Nd). The intermetallic phase was identified as low-temperature orthorhombic $\alpha Al_{11}X_3$ for Al–6Nd and Al–9Ce and for Zone B of Al–22Ce. For Zone A in Al–16Nd and Al–22Ce it was not possible to distinguish between the tetragonal high-temperature modification and the orthorhombic low-temperature modification of the $Al_{11}X_3$.

2. The microstructure of the as-spun ribbons changed from a fully Zone B structure to a fully Zone A structure when the content of neodymium was increased from 6 wt% to 16 wt%. For Al–Ce, increasing the cerium content from 9 wt% to 22 wt% gave a partial change from fully Zone B to Zone A, plus Zone B and a few fully lamellar eutectic areas. The lamellar eutectic consisted of αAl and $\alpha Al_{11}Ce_3$ with an orientation relationship $\langle 0\,0\,1\rangle \alpha Al \parallel [0\,1\,0]$ $\alpha Al_{11}Ce_3$ and $\{2\,0\,0\}$ αAl ∥ (0 0 2) $\alpha Al_{11}Ce_3$.

3. No evidence for any substantial extension of the solid solubility of neodymium and cerium in αAl was found and age hardening was not observed in any of the melt-spun ribbons as a result of 2 h heat treatments in the range 200–500 °C.

4. The Knoop microhardness as-spun increased with increasing alloying content. The as-spun ribbons which had a Zone A structure showed the highest hardness. The hardness of Al–16Nd was 330 ± 20 HK0.01, this value being unchanged by treatment at 200 °C for 2 h. Heat treatments at higher temperatures (300–500 °C for 2 h) caused a decrease in hardness. The hardness of Al–6Nd and Al–9Ce ribbons was unchanged at 75–80 HK0.01 and 90 HK0.01, respectively, by treatments for 2 h at 200 or 300 °C and showed a decrease on heat treatment at higher temperatures.

5. TEM investigation of the ribbons heat treated at 500 °C for 2 h showed a coarsened bimodal distribution of intermetallic particles for all the alloys. The intermetallic phases were identified by XRD to be the orthorhombic low-temperature α-variant of $Al_{11}X_3$ (X = Ce or Nd) for all the alloys investigated.

Acknowledgement

Grethe Waterloo is grateful for financial support from the Norwegian Research Council that enabled her to carry out this work at the University of Sheffield.

References

1. S. J. SAVAGE and F. H. FROES, in "Rapidly Solidified Metastable Materials", edited by B. H. Kear and B. C. Giessen (Elsevier Science, New York, 1984) p. 329.
2. S. J. SAVAGE and Y. R. MAHAJAN, in "Rapidly Quenched Metals", edited by S. Steeb and H. Warlimont (Elsevier North Holland, Amsterdam, 1985) p. 915.
3. S. J. SAVAGE, F. H. FROES and D. ELIEZER, in "Rapidly Solidified Materials", edited by P. W. Lee and R. S. Carbonara (ASM International Metals Park, OH, 1985) p. 351.
4. D. ELIEZER, S. J. SAVAGE, Y. R. MAHAJAN and F. H. FROES, in "Rapidly Solidified Alloys and their Mechanical and Magnetic Properties", edited by B. C. Giessen, D. E. Polk and A. I. Taub (MRS, Pittsburgh, PA, 1986) p. 293.
5. S. J. SAVAGE, D. ELIEZER and F. H. FROES, *Metall. Trans.* **18A** (1987) 1533.
6. M. FASS, D. ITZHAK, D. ELIEZER and F. H. FROES, *J. Mater. Sci. Lett.* **6** (1987) 1227.
7. A. RUDER and D. ELIEZER, *Israel J. Technol.* **24** (1988) 149.
8. M. FASS, D. ITZHAK, D. ELIEZER and F. H. FROES, *J. Mater. Sci. Lett.* **7** (1988) 76.
9. D. ELIEZER, M. FASS, D. ITZHAK, Y.-W. KIM and F. H. FROES, in "Rapidly Solidified Materials: Properties and Processing", edited by P. W. Lee and J. H. Moll (ASM International, Metals Park, OH, 1988) p. 83.
10. A. RUDER and D. ELIEZER, *J. Mater. Sci.* **24** (1989) 1474.
11. M. FASS and D. ELIEZER, *J. Mater. Sci. Lett.* **8** (1989) 178.
12. A. RUDER and D. ELIEZER, *ibid.* **8** (1989) 725.
13. *Idem., J. Mater. Sci.* **25** (1990) 3541.
14. A. INOUE, K. OHTERA and T. MASUMOTO, *Jpn. J. Appl. Phys.* **27** (1988) L736.
15. A. INOUE, K. OHTERA, Z. TAO and T. MASUMOTO, *ibid.* **27** (1988) L1583.
16. A. INOUE, T. ZHANG, K. KITA and T. MASUMOTO, *Mater. Trans. JIM* **30** (1989) 870.
17. A. INOUE, K. OHTERA and T. MASUMOTO, *Sci. Rep. RITU A* **35** (1990) 115.
18. A. INOUE, M. WATANABE, H. KIMURA and T. MASUMOTO, *ibid.* **36** (1991) 59.

19. B. DILL, Y. LI, M. Al-KHAFAJI, W. M. RAINFORTH, R. A. BUCKLEY and H. JONES, *J. Mater. Sci.* **29** (1994) 3913.
20. M. A. AL-KHAFAJI, Y. LI, W. M. RAINFORTH and H. JONES, *Philos. Mag. B* **70** (1994) 1129.
21. H. JONES, *Mater. Sci. Eng.* **5** (1969) 1.
22. K. H. J. BUSCHOW and J. H. N. VAN VUCHT, *Z. Metallkde* **57** (1996) 162.
23. H. NOWOTNY, *Z. Kristallogr.* **34** (1942) 22.
24. K. H. J. BUSCHOW, *J. Less-Common Metals* **9** (1965) 452.
25. P. I. KRIPYAKEVICH and E. I. GLADYSHEVSKII, *Sov. Phys. Crystallogr.* **6** (1961) 95.
26. W. B. PEARSON, "A Handbook of Lattice Spacings and Structures of Metals and Alloys" (Pergamon, Oxford, 1964).
27. Y. NING, X. SHOU and H. DAI, *Acta Metall. Sin* **28** (3) (1992) B95.
28. K. A. GSCHNEIDNER Jr and F. W. CALDERWOOD, *Bull. Alloy Phase Diagrams* **9** (1988) 669.
29. *Idem., ibid.* **10** (1989) 28.
30. H. OKAMOTO, *J. Phase Equilib.* **12** (1991) 500.
31. K. A. GSCHNEIDNER Jr and F. W. CALDERWOOD, *Bull. Alloy. Phase Diagrams* **9** (1988) 658.
32. W. J. BOETTINGER, D. SHECHTMAN, R. J. SCHAEFER and F. S. BIANCANIELLO, *Metall. Trans.* **15A** (1984) 55.
33. H. JONES, *Mater. Lett.* **6** (1988) 181.
34. *Idem*, "Rapid Solidification of Metals and Alloys" (Institution of Metallurgists, London, 1982).
35. J. E. HATCH, "Aluminium – Properties and Physical Metallurgy" (ASM, Metals Park, OH, 1984).
36. K. N. STREET, C. F. ST JOHN and G. PIATTI, *J. Inst. Metals* **95** (1967) 326.

Received 8 August
and accepted 7 November 1995